

# Kondo and Majorana signatures near the singlet-doublet quantum phase transition

G. Górski,<sup>1</sup> J. Barański,<sup>2</sup> and T. Domański<sup>3,\*</sup>

<sup>1</sup>*Faculty of Mathematics and Natural Sciences, University of Rzeszów, 35-310 Rzeszów, Poland*

<sup>2</sup>*Institute of Physics, Polish Academy of Sciences, 02-668 Warsaw, Poland*

<sup>3</sup>*Institute of Physics, M. Curie-Skłodowska University, 20-031 Lublin, Poland*

(Dated: June 22, 2019)

We study the low energy quasiparticles driven by the Kondo effect and the proximity induced Majorana state in a setup, comprising the correlated quantum dot coupled between the conducting and superconducting reservoirs and additionally hybridized with the topological superconducting nanowire. We investigate mutual interplay of the Kondo and Majorana states appearing near the quantum phase transition/crossover from the (spinless) BCS-type singlet to the (spinful) doublet ground states. We find novel properties, stemming from the subgap Kondo effect combined with the Majorana quasiparticle and discuss their signatures in the tunneling conductance, originating from the particle-to-hole (Andreev scattering) mechanism.

## I. INTRODUCTION

Recently there has been enormous activity devoted to quasiparticles, resembling the Majorana fermions [1–5] that are identical with their own antiparticles. Such exotic objects have been predicted at topological defects [6] or at boundaries of the symmetry broken systems [7, 8] and their non-Abelian character could be useful for the quantum computing and/or novel spintronic devices [9]. Although such Majorana quasiparticles has been predicted in various systems [10–20], their experimental realization has been so far observed in the ballistic tunneling [21, 22] and in STM measurements [23–26] via nanowires proximity-coupled to the bulk *s*-wave superconductors.

Inspired by the work by M.T. Deng *et al.* [27], who provided experimental evidence for the Majorana modes leaking onto the quantum dot side-attached to InAs nanowire in its topologically nontrivial superconducting state, we consider the setup (displayed in Fig. 1) studying interplay between the Kondo effect and Majorana quasiparticle (both manifested near the zero energy). Andreev states coalescing into the zero-energy Majorana state have been discussed at length by several authors [28–30], but influence of the correlations has been addressed on the Hartree-Fock level [31], the equation of motion approach [32], or by means of NRG [33] for very weak coupling  $\Gamma_N$  to the conducting lead. Our present study focuses on the subgap Kondo effect, originating in the proximitized and correlated quantum dot solely due to this coupling. Such situation could be realized in STM-type geometry, similar to what has been used by the Princeton [23] and Basel [24] groups. We thus propose to use a nanoscopic chain of magnetic atoms (e.g. Fe) with one (or a few) side-coupled nonmagnetic atoms (for instance Ag or Au) deposited on the superconducting substrate (like Pb) and probed either by the normal or ferromagnetic STM tip. The latter possibility has been recently achieved by A. Yazdani and coworkers [26].

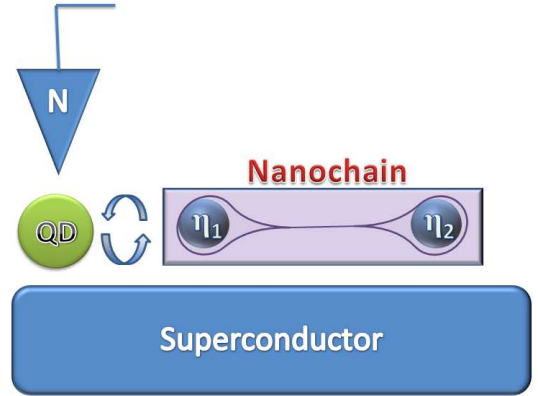


FIG. 1. Schematic illustration of the quantum dot (QD) laterally coupled to the metallic (N) and superconducting (S) electrodes and additionally hybridized with the Rashba nanowire, hosting the Majorana quasiparticles  $\eta_1$  and  $\eta_2$  at its edges.

We thus analyze the quantum dot (QD) placed between a superconducting (S) and metallic (N) lead and side-coupled to the Rashba nanowire, hosting the Majorana quasiparticles at its ends (Fig. 1). This N-QD-S setup hybridized with the Majorana quasiparticle has a geometry of *T-shape* junction. We shall investigate here the Majorana quasiparticle near the quantum phase transition/crossover from the (spinless) BCS-type to the (spinfull) singly occupied ground state [34], studying its interplay with the Kondo effect and electron pairing.

Similar configurations with two metallic [35–43] or ferromagnetic [44, 45] electrodes have been studied by other groups. It was found that the Majorana quasiparticle „leaking” into the QD region strongly affects the Kondo resonance. Its influence could be observed in the linear conductance. It was established that for infinitely long chain (where overlap between Majorana end-modes is absent) the linear conductance reaches  $3e^2/2h$ , whereas in the case of short chain (with nonzero overlap between Majoranas) the conductance peak reaches  $2e^2/h$  [36, 37, 44, 45]. Further analysis of the thermoelectric properties of such N-QD-N setup revealed that for small overlap the thermopower reverses its sign [36, 44, 45].

\* e-mail: doman@kft.umcs.lublin.pl

Such *T-shape* junctions with one normal and one superconducting electrode have been much less explored [32, 33, 40, 46]. Owing to the proximity effect electrons of the QD are bound in pairs [47, 48], so physical processes engaging electrons of a given spin would simultaneously affect its opposite spin partner [49]. In particular, the side-attached Majorana quasiparticle hybridized with, let's say,  $\uparrow$  electron affects the energy spectrum of  $\downarrow$  electrons. Consequently, both spin channels become interdependent. This effect is particularly important when considering the Andreev processes, in which both of the spin components equally participate in the subgap transport process.

The paper is organized as follows. In Sec. II we formulate the microscopic model. Next, in Sec. III we study effects appearing in a subgap spectrum and in tunneling conductance of the uncorrelated QD. Sections IV and V discuss the correlation effects in the superconducting atomic limit and the Kondo regime, respectively. In Sec. VI we summarize the main results additional data for the short Rashba wire are presented in Appendix A.

## II. LOW ENERGY MODEL

Empirical realizations of the topological superconductivity in the semiconducting wires [21, 22] or magnetic atoms' chain [23–26] rely on the *p*-wave pairing (of identical spins) between the nearest neighbor sites, reminiscent of the Kitaev scenario [8]. In this paper we assume that such pairing is induced for  $\uparrow$  electrons, so only this particular spin component of QD is *directly* coupled to the Majorana quasiparticle [39, 50]. Due to the proximity induced on-dot pairing, however, the other ( $\downarrow$ ) spin is *indirectly* influenced by the Majorana quasiparticle as well. For this reason, any process engaging  $\uparrow$  electrons would simultaneously (although with different efficiency) affect the opposite spin [49]. This would be very important for the Andreev (particle to hole conversion) scattering, which is the only subgap transport channel at low temperatures.

Our setup (Fig. 1) can be described by the following Anderson-type Hamiltonian

$$H = \sum_{\beta=S,N} (H_{\beta} + H_{\beta-QD}) + H_{QD} + H_{MQD}, \quad (1)$$

$$\mathcal{G}^{-1}(\omega) = \begin{pmatrix} \omega - \epsilon + i\Gamma_N/2 & \Gamma_S/2 & -t_m & -t_m \\ \Gamma_S/2 & \omega + \epsilon + i\Gamma_N/2 & 0 & 0 \\ -t_m & 0 & \omega - \epsilon_m - t_m^2/b & -t_m^2/b \\ -t_m & 0 & -t_m^2/b & \omega + \epsilon_m - t_m^2/b \end{pmatrix}, \quad (4)$$

where  $b = \omega + \epsilon + i\Gamma_N/2 - (\Gamma_S/2)^2/(\omega - \epsilon + i\Gamma_N/2)$ . For  $\epsilon_m = 0$  (i.e. without any overlap between the Majorana fermions) the Greens function can be expressed explicitly

where  $H_N = \sum_{k,\sigma} \xi_{kN} c_{k\sigma N}^{\dagger} c_{k\sigma N}$  describes the metallic electrode,  $H_S = \sum_{k,\sigma} \xi_{kS} c_{k\sigma S}^{\dagger} c_{k\sigma S} - \sum_k (\Delta c_{k\uparrow S}^{\dagger} c_{-k\downarrow S}^{\dagger} + h.c.)$  refers to *s*-wave superconducting substrate and electron energies  $\xi_{k\beta}$  are measured with respect to the chemical potentials  $\mu_{\beta}$ . The correlated QD is described by  $H_{QD} = \sum_{\sigma} \epsilon d_{\sigma}^{\dagger} d_{\sigma} + U n_{\downarrow} n_{\uparrow}$ , where  $\epsilon$  denotes the energy level and  $U$  stands for the repulsive interaction between opposite spin electrons. The QD is coupled to both external reservoirs via  $H_{\beta-QD} = \sum_{k,\sigma} (V_{k\beta} d_{\sigma}^{\dagger} c_{k\sigma\beta} + h.c.)$ , where  $V_{k\beta}$  denote the matrix elements. In a wide bandwidth limit, it is convenient to introduce the auxiliary couplings  $\Gamma_{\beta} = 2\pi \sum_k |V_{k\beta}|^2 \delta(\omega - \xi_{k\beta})$ , which we assume to be constant. For energies  $|\omega| \ll \Delta$  it has been shown [51–54] that the superconducting electrode induces the static pairing  $H_S + H_{S-QD} \approx H_{prox} = \sum_{\sigma} \epsilon d_{\sigma}^{\dagger} d_{\sigma} + U n_{\downarrow} n_{\uparrow} - \frac{\Gamma_S}{2} (d_{\uparrow} d_{\downarrow} + d_{\downarrow}^{\dagger} d_{\uparrow}^{\dagger})$ . We make use of this low energy model, whose extension on the realistic  $\Delta$  has been widely discussed in the literature 28.

The zero-energy end modes of the topological nanowire can be modeled by the following term [41]

$$H_{MQD} = i\epsilon_m \eta_1 \eta_2 + \lambda (d_{\uparrow} \eta_1 + \eta_1 d_{\uparrow}^{\dagger}) \quad (2)$$

with the Majorana (selfhermitian) operators  $\eta_i = \eta_i^{\dagger}$ , where  $\epsilon_m$  corresponds to their overlap. We recast these Majorana by the standard fermionic operators [5]  $\eta_1 = \frac{1}{\sqrt{2}}(f + f^{\dagger})$  and  $\eta_2 = \frac{i}{\sqrt{2}}(f - f^{\dagger})$  so that the term (2) can be expressed as

$$H_{MQD} = t_m (d_{\uparrow}^{\dagger} - d_{\uparrow})(f + f^{\dagger}) + \epsilon_m f^{\dagger} f + \frac{\epsilon_m}{2}, \quad (3)$$

where  $t_m = \lambda/\sqrt{2}$ .

## III. MAJORANA VS ELECTRON PAIRING

We first consider the case of uncorrelated QD ( $U = 0$ ). Let us calculate the Green's function  $\mathcal{G}(\omega) = \langle\langle \Psi; \Psi^{\dagger} \rangle\rangle$  in the following matrix notation  $\Psi = (d_{\uparrow}, d_{\downarrow}^{\dagger}, f, f^{\dagger})$

by

$$\mathcal{G}_{11}(\omega) = \frac{\omega + \epsilon + i\frac{\Gamma_N}{2}}{D_1(\omega)} + \frac{2t_m^2(\omega + \epsilon + i\frac{\Gamma_N}{2})^2}{D(\omega)}, \quad (5)$$

$$\mathcal{G}_{22}(\omega) = \frac{\omega - \epsilon + i\frac{\Gamma_N}{2}}{D_1(\omega)} + \frac{2t_m^2(\frac{\Gamma_S}{2})^2}{D(\omega)}, \quad (6)$$

$$\mathcal{G}_{12}(\omega) = \frac{-\frac{\Gamma_S}{2}}{D_1(\omega)} - \frac{2t_m^2(\omega + \epsilon + i\frac{\Gamma_N}{2})\frac{\Gamma_S}{2}}{D(\omega)}, \quad (7)$$

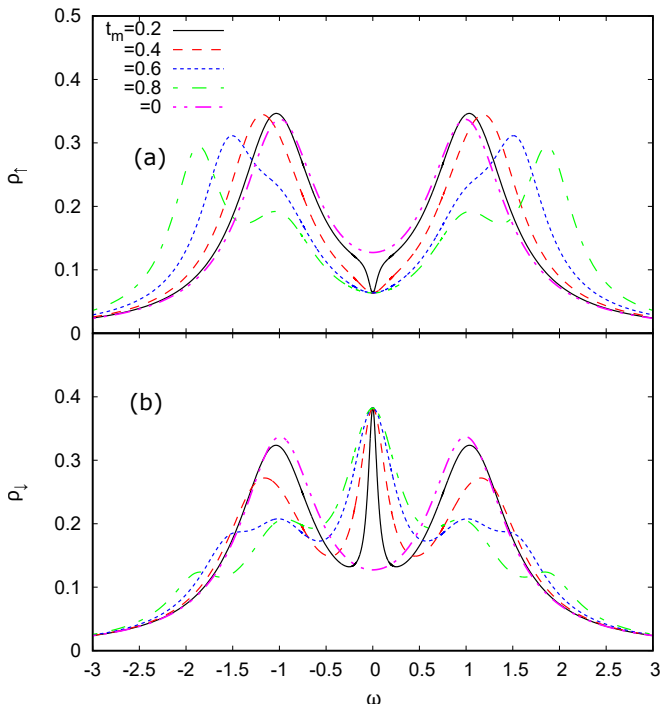


FIG. 2. Spectral function  $\rho_\sigma(\omega)$  of the uncorrelated dot  $U = 0$  obtained for  $\Gamma_S = 2\Gamma_N$ ,  $\epsilon = 0$  and various couplings  $t_m$ .

where  $D(\omega) \equiv D_1(\omega)[\omega D_1(\omega) - 4t_m^2(\omega + i\Gamma_N/2)]$  and  $D_1(\omega) \equiv (\omega + i\Gamma_N/2)^2 - \epsilon^2 - (\Gamma_S/2)^2$ . These Green's functions (5)-(7) are composed of the part, representing solution for the quantum dot coupled only to N and S electrodes ( $t_m = 0$ ) (first terms of r.h.s Eqs. (5)-(7)) and additional term dependent on coupling to the Majorana fermions. In the *SC atomic limit*,  $\Gamma_N \rightarrow 0$ , such Green's function is characterized by five poles: two of them corresponding to the Andreev bound states ( $\pm\sqrt{\epsilon^2 + (\Gamma_S/2)^2}$ ) and three additional states resulting from the Majorana fermions ( $0, \pm\sqrt{\epsilon^2 + (\Gamma_S/2)^2 + (2t_m)^2}$ ). The correlation effects shall be discussed in sections IV and V.

### A. Free quasiparticle spectrum

Fig. 2 shows the spin-resolved spectral function  $\rho_\sigma(\omega)$  of the uncorrelated QD obtained at half-filling ( $\epsilon = 0$ ) for various couplings  $t_m$ . As a reference shape we also present the spectrum in absence of the Majorana quasiparticles ( $t_m = 0$ ), revealing the Andreev quasiparticle peaks at  $\omega = \pm\sqrt{\epsilon^2 + (\Gamma_S/2)^2}$  whose broadening is  $\Gamma_N$ . For  $t_m \neq 0$  the spin-resolved spectra are no longer identical due to the direct (indirect) coupling of  $\uparrow$  ( $\downarrow$ ) QD electrons with the side-attached Majorana state. The most significant differences show up near  $\omega \sim 0$ . In particular, direct hybridization of  $\uparrow$  electrons depletes their spectrum near the Majorana state. Exactly at  $\omega = 0$  their spectral function is reduced by half,  $\rho_\uparrow(0)|_{t_m \neq 0} = 0.5\rho_\uparrow(0)|_{t_m = 0}$ , similarly to what has been reported for the same ge-

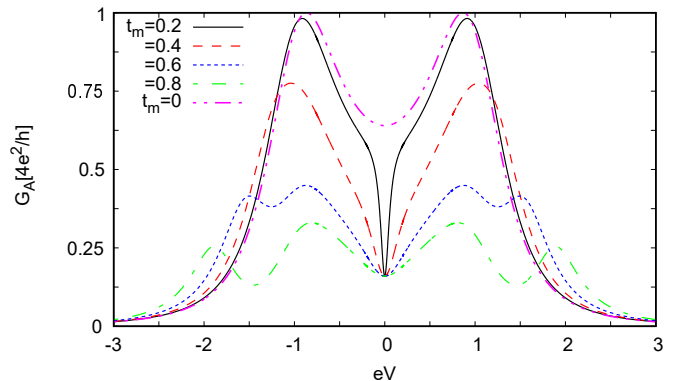


FIG. 3. The differential Andreev conductance obtained at zero temperature for the same model parameters as in Fig. 2.

ometry with both nonsuperconducting leads [37, 44, 50]. Contrary to this behavior, the spin  $\downarrow$  electrons (indirectly coupled to the Majorana state via on-dot pairing) clearly gain the electronic states. Again, at  $\omega = 0$  the spectral function  $\rho_\downarrow(0)$  does not depend on  $t_m$  (unless  $t_m$  vanishes). This constructive feedback of the side-attached Majorana state on  $\downarrow$  electrons has no analogy to any normal systems [37, 44, 50].

Upon increasing the coupling  $t_m$  we observe a gradual splitting of the Andreev quasiparticles, leading to emergence of the effective *molecular* structure. We can notice some differences appearing in the spectrum  $\rho_\sigma(\omega)$  of  $\uparrow$  and  $\downarrow$  electrons, especially in the low energy region.

### B. Quasiparticle features in tunneling spectroscopy

Low energy quasiparticles of the QD, which is side-attached to the Majorana mode, can be probed in our setup (Fig. 1) only indirectly, via the tunneling current. When voltage  $V$  applied between the normal tip and superconducting substrate is smaller than the energy gap  $\Delta$  the charge transport can be provided solely by the Andreev reflections [55]. Such transport channel can be described quantitatively by the Landauer expression

$$I_A(V) = \frac{e}{h} \int d\omega T_A(\omega) [f(\omega - eV) - f(\omega + eV)], \quad (8)$$

where  $f(x) = [1 + \exp(x/k_B T)]^{-1}$  is the Fermi distribution. The energy-dependent transmittance

$$T_A(\omega) = \Gamma_N^2 \left| \mathcal{G}^{(12)}(\omega) \right|^2 + \Gamma_N^2 \left| \mathcal{G}^{(21)}(\omega) \right|^2 \quad (9)$$

describes probability that an electron (from STM tip) with spin  $\sigma$  is converted into a hole (reflected back to the STM tip) with an opposite spin  $\bar{\sigma}$ , injecting one Cooper pair into the superconducting substrate. It has been previously emphasized [54], that the differential conductance  $G_A(V) = dI_A(V)/dV$  can detect the sub-gap quasiparticle states, at expense of mixing the particle and with hole degrees of freedom. In particular, at

zero temperature the differential conductance simplifies to  $G_A(V) = \frac{2e^2}{h} [T_A(\omega = +eV) + T_A(\omega = -eV)]$ .

Fig. 3 shows the differential Andreev conductance obtained at zero temperature for different values of  $t_m$ , assuming  $\epsilon_m = 0$ . We observe, that for all finite couplings  $t_m \neq 0$  the linear conductance  $G_A(V=0)$  drops to the value  $\frac{1}{4}G_A(V=0)_{t_m=0}$ . This result is qualitatively different from what have been obtained for N-QD-N junctions, where  $G(V=0)_{t_m \neq 0} = \frac{3}{4}G(V=0)_{t_m=0}$  (see Ref. 37). Upon increasing the coupling  $t_m$  the nonlinear conductance  $G_A(V \neq 0)$  develops four local maxima, two of them at  $\pm\sqrt{\epsilon^2 + (\Gamma_S/2)^2}$  and additional pair at  $\pm\sqrt{\epsilon^2 + (\Gamma_S/2)^2 + (2t_m)^2}$ . These local maxima are no longer equal to the perfect Andreev conductance  $4e^2/h$ . They originate from the bonding/antibonding Andreev states combined with the Majorana quasiparticle (see Fig. 2).

#### IV. MAJORANA STATE NEAR THE SINGLET-DOUBLET TRANSITION

To gain some insight into the correlation effects let us first consider the strongly asymmetric limit  $\Gamma_S \gg \Gamma_N$ , assuming  $\Gamma_N = 0^+$ . Influence of the Coulomb repulsion  $U$  on the subgap Andreev states in the large gap  $\Delta$  limit with a vanishing coupling to the normal lead has been first addressed by E. Vecino *et al* [56]. The effective bound states of this *superconducting atomic limit* have been discussed in the review paper 57. In the present context we consider the proximitized QD coupled to the Majorana modes, i.e.

$$\hat{H} \simeq \sum_{\sigma} \epsilon d_{\sigma}^{\dagger} d_{\sigma} + U n_{\downarrow} n_{\uparrow} - \frac{\Gamma_S}{2} (d_{\uparrow} d_{\downarrow} + d_{\downarrow}^{\dagger} d_{\uparrow}^{\dagger}) + t_m (d_{\uparrow}^{\dagger} - d_{\uparrow})(f + f^{\dagger}) + \epsilon_m \left( f^{\dagger} f + \frac{1}{2} \right). \quad (10)$$

From now onwards we introduce the shorthand notations for the induced pairing gap  $\Delta_d \equiv \frac{\Gamma_S}{2}$  and for the shifted QD level  $\xi_d \equiv \epsilon + \frac{U}{2}$ , respectively.

In absence of the hybridization  $t_m$  the true eigenstates of QD are represented by the doublet configurations  $|\uparrow\rangle$  and  $|\downarrow\rangle$  (corresponding to QD spin  $S = \frac{1}{2}$ ) and the BCS-like singlet states ( $S = 0$ )

$$|\Psi_{-}\rangle = u_d |0\rangle - v_d |\uparrow\downarrow\rangle, \quad (11)$$

$$|\Psi_{+}\rangle = v_d |0\rangle + u_d |\uparrow\downarrow\rangle. \quad (12)$$

with the eigenenergies  $E_{\mp} = \xi_d \mp \sqrt{\xi_d^2 + \Delta_d^2}$  and the coefficients  $u_d^2 = \frac{1}{2} \left[ 1 + \frac{\xi_d}{E_d} \right] = 1 - v_d^2$ , where  $E_d = \sqrt{\xi_d^2 + \Delta_d^2}$ . In the present case, however, we have to extend the Hilbert space by the additional fermion state  $f$  (which can be either empty or occupied). We have numerically diagonalized the Hamiltonian matrix in the occupancy representation  $|n_{d\uparrow}\rangle \otimes |n_{d\downarrow}\rangle \otimes |n_f\rangle$ , determining the eigenvalues and eigenvectors. Using the spectral (Lehmann)

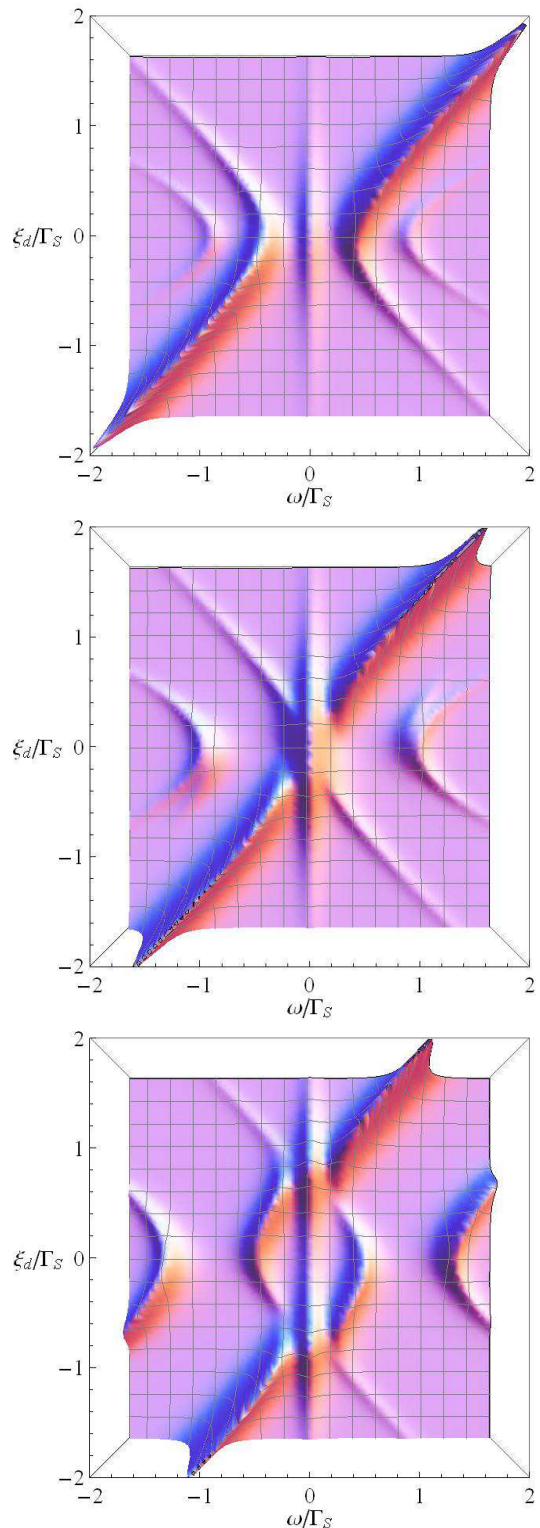


FIG. 4. The spectral function  $\rho_r(\omega)$  of the correlated and proximitized QD obtained for  $t_m = 0.3\Gamma_S$ ,  $\Gamma_N \rightarrow 0$ , using  $U = 0.05\Gamma_S$  (top panel),  $1\Gamma_S$  (middle panel), and  $2\Gamma_S$  (bottom panel). Calculations are done by exact numerical diagonalization of the Hamiltonian (10) and imposing a small line broadening.

representation we have computed the spectral functions and calculated the Andreev transmittance.

Fig. 4 shows the QD spectrum for three representative values of the Coulomb potential. In the weak interaction limit (top panel) the spectrum exhibits the non-crossing Andreev quasiparticle branches coexisting with the zero-energy mode leaking into the QD. For  $U = \Gamma_S$  we observe a tendency towards the Andreev bound states crossing at  $\xi_d \sim 0$  ( $\epsilon \sim -\frac{U}{2}$ ). However, due to hybridization with the Majorana mode, we rather observe emergence of the three-peak (*molecular*) structure. In the strong correlation case  $U = 2\Gamma_S$  (bottom panel) there appear two crossing points aside from the half-filling [51], but we still can see the 3-peak spectrum. This behavior shows that quantum phase transition from the (spinful) doublet to the (spinless) BCS-type configurations is obscured by a leakage of the Majorana mode. Actually, the Majorana and Andreev modes give rise to the novel 3-peak structure. In section V we shall examine possible formation of the subgap Kondo effect.

## V. MAJORANA VS KONDO

Now, we analyze the correlated quantum dot taking into account the finite coupling  $\Gamma_N$  to the normal STM tip. It has been recently shown [58, 59], that in absence of the Majorana quasiparticle the induced on-dot pairing cooperates with the Coulomb repulsion, enhancing the subgap Kondo effect. Its spectroscopic observation is possible only nearby the quantum phase transition, on the (spinful) doublet side.

Our main purpose here is to examine how this subgap Kondo effect (usually appearing at zero energy) gets along with the leaking Majorana mode. Some earlier studies of the correlated quantum dot coupled to both normal (conducting) electrodes in presence of the side-attached Rashba chain indicated a competition between the Kondo and Majorana physics [37, 44, 45, 50, 60, 61]. For sufficiently long wire ( $\epsilon_m = 0$ ) the Kondo effect is preserved only for the spin-channel  $\downarrow$  (which is not coupled to the Majorana zero-energy mode), whereas for the other spin-channel  $\uparrow$  there appears a dip in the spectral density at  $\omega = 0$  (reminiscent to what we observed in the upper panel of Fig. 2). In consequence, the total transmission is partly blocked suppressing the linear conductance from  $2e^2/h$  to the fractional value  $3e^2/2h$  [36, 37, 44, 45, 50]. For the short Rashba wires ( $\epsilon_m \neq 0$ ) the Kondo physics survives in both of the spin channels, but a width of the Abrikosov-Suhl peak depends on  $\epsilon_m$ . The initial Kondo features are fully recovered in both spin-channels only when  $\epsilon_m \gg (|\epsilon|, U, \Gamma)$ . Results for the short length Rashba wires are shown in Appendix A.

When the correlated quantum dot is embedded between the metallic and superconducting leads (N-QD-S) the eventual subgap Kondo effect is controlled by  $U/\Gamma_S$  ratio and  $\epsilon$ , which decide whether the ground-state is either the (spinful) doublet or the (spinless) BCS-type

configuration [34, 52, 54, 58, 62]. In particular, for the half-filled QD ( $\epsilon = -\frac{U}{2}$ ) the BCS singlet exists in the weak correlation regime  $U < \Gamma_S$ , whereas the doublet is preferred in the strongly correlated limit  $U > \Gamma_S$ . In the latter case the Kondo temperature eventually occurs, and moreover the effective Kondo temperature can be amplified by the increasing coupling strength  $\Gamma_S$  [58, 59].

In the present setup the Coulomb interactions (responsible for the Kondo effect) are additionally confronted with the Majorana physics. To study such effects qualitatively we compute the self-energy  $\Sigma(\omega)$  of the matrix Green's function (4), treating the Coulomb interaction perturbatively. Formally we solve the Dyson equation  $\mathcal{G}_{U \neq 0}^{-1}(\omega) = \mathcal{G}_{U=0}^{-1}(\omega) - \Sigma(\omega)$ , adopting the second-order perturbation theory (SOPT) [52, 56, 58]

$$\begin{aligned} \Sigma_{11}(\omega) &= U \langle d_{\downarrow}^{\dagger} d_{\downarrow} \rangle \\ &+ U^2 \int_{-\infty}^{\infty} \frac{-\frac{1}{\pi} \text{Im} \Sigma_{11}^{(2)}(\omega')}{\omega - \omega' + i0^+} d\omega', \end{aligned} \quad (13)$$

$$\begin{aligned} \Sigma_{22}(\omega) &= U \langle d_{\uparrow}^{\dagger} d_{\uparrow} \rangle \\ &+ U^2 \int_{-\infty}^{\infty} \frac{-\frac{1}{\pi} \text{Im} \Sigma_{22}^{(2)}(\omega')}{\omega - \omega' + i0^+} d\omega', \end{aligned} \quad (14)$$

$$\begin{aligned} \Sigma_{12}(\omega) &= U \langle d_{\downarrow} d_{\uparrow} \rangle \\ &- U^2 \int_{-\infty}^{\infty} \frac{-\frac{1}{\pi} \text{Im} \Sigma_{12}^{(2)}(\omega')}{\omega - \omega' + i0^+} d\omega'. \end{aligned} \quad (15)$$

The imaginary parts of the second-order contributions  $\Sigma_{ij}^{(2)}(\omega)$  are expressed by the following convolutions [59]

$$\begin{aligned} -\frac{1}{\pi} \text{Im} \Sigma_{11(22)}^{(2)}(\omega) &= \int_{-\infty}^{\infty} \left[ \mathbf{\Pi}_1(\omega + \omega') \rho_{22(11)}^+(\omega') \right. \\ &\quad \left. + \mathbf{\Pi}_2(\omega + \omega') \rho_{22(11)}^-(\omega') \right] d\omega', \quad (16) \\ -\frac{1}{\pi} \text{Im} \Sigma_{12}^{(2)}(\omega) &= \int_{-\infty}^{\infty} \left[ \mathbf{\Pi}_1(\omega + \omega') \rho_{21}^+(\omega') \right. \\ &\quad \left. + \mathbf{\Pi}_2(\omega + \omega') \rho_{21}^-(\omega') \right] d\omega', \quad (17) \end{aligned}$$

where

$$\begin{aligned} \mathbf{\Pi}_{1(2)}(\omega) &= \int_{-\infty}^{\infty} \left[ \rho_{11}^{-(+)}(\omega') \rho_{22}^{-(+)}(\omega - \omega') \right. \\ &\quad \left. - \rho_{12}^{-(+)}(\omega') \rho_{21}^{-(+)}(\omega - \omega') \right] d\omega', \quad (18) \end{aligned}$$

and the auxiliary functions  $\rho_{ij}^{\pm}(\omega) \equiv \frac{-1}{\pi} \text{Im} \mathcal{G}^{ij}(\omega + i0^+) f(\pm\omega)$  denote the occupancies obtained from the uncorrelated Green's functions (4), but taking into account the effective dot level and the effective superconducting coupling strength [52].

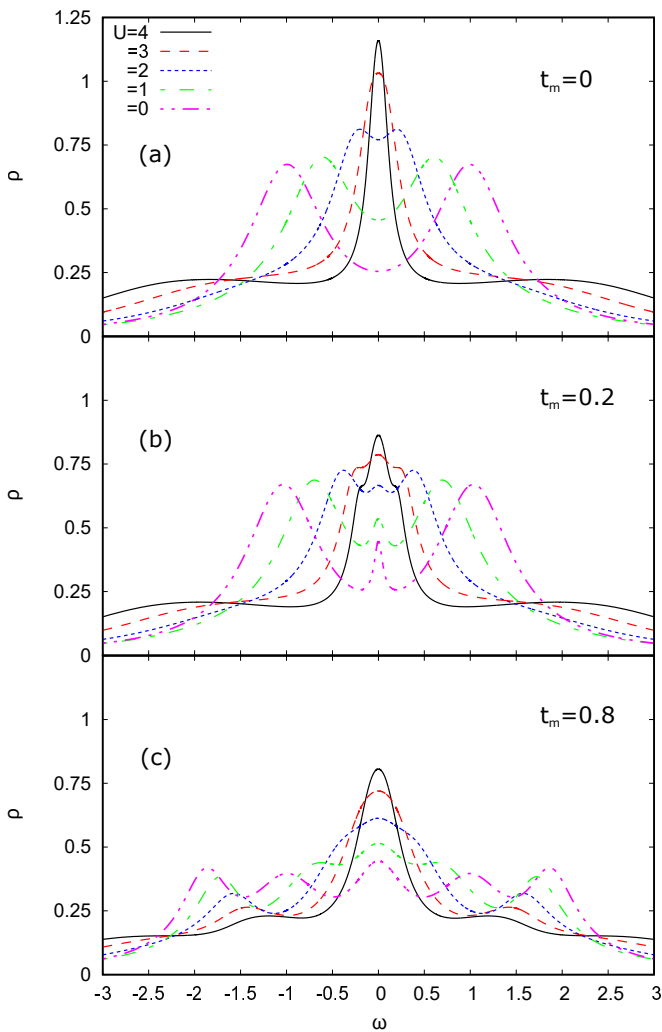


FIG. 5. The total spectral function  $\rho(\omega) = \sum_{\sigma} \rho_{\sigma}(\omega)$  of the half-filled quantum dot ( $\varepsilon = -U/2$ ) obtained at  $T = 0$  for  $\Gamma_S = 2\Gamma_N$  and several values of the Coulomb potential  $U$  (as indicated), assuming (a)  $t_m = 0$ , (b)  $t_m = 0.2$ , and (c)  $t_m = 0.8$ . All energies are expressed in units of  $\Gamma_N$ .

In what follows we discuss the total spectral function  $\rho(\omega) = \sum_{\sigma} \rho_{\sigma}(\omega)$ , because empirical detection (by the Andreev spectroscopy) would mix the quasiparticles of both spin orientations. Fig. 5 shows  $\rho(\omega)$  obtained at zero temperature for various Coulomb potentials, as indicated. The top panel refers to N-QD-S system without any coupling to the Majorana mode. In the weak interaction regime it reveals two Andreev peaks. Upon approaching  $U \approx \Gamma_S$  these peaks merge, signaling the quantum phase transition (for  $\Gamma_N \neq 0$  it becomes a continuous crossover). In the strongly correlated limit ( $U > \Gamma_S$ ), the Kondo peak develops at  $\omega = 0$  and its broadening gradually shrinks upon increasing the ratio  $U/\Gamma_S$  [52, 58].

Coupling of the correlated QD to the Majorana mode (whose spectrum is displayed in panels b and c of Fig. 5) leads to appearance of additional structure near  $\omega \approx 0$ , even for  $U = 0$ . A width of this additional structure is controlled by  $t_m$ . Upon increasing  $U$  it becomes hardly

distinguishable from Andreev peaks, forming a single broad peak. For the sufficiently strong Coulomb potential the spectral function at  $\omega = 0$  tends to  $\rho(0)_{t_m} \approx \frac{3}{4}\rho(0)_{t_m=0}$ . Similar result has been previously obtained from NRG calculations for the quantum dot - Majorana system coupled to both ferromagnetic electrodes [45].

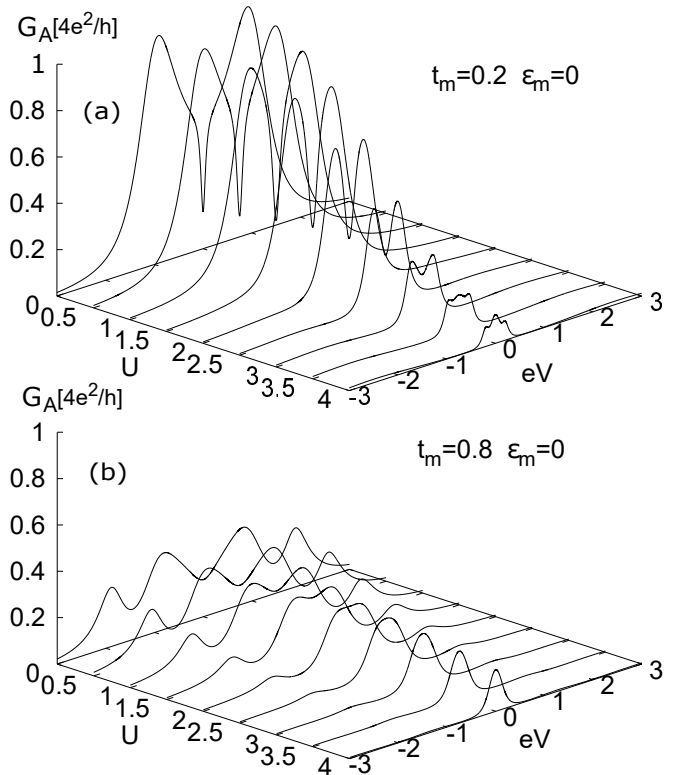


FIG. 6. The differential subgap conductance  $G_A(V)$  as a function of the applied voltage obtained for the same set of parameters as in figure 5.

Practical observation of the above mentioned effects would be accessible by measuring the subgap current (8). Fig. 6 shows the Andreev conductance  $G_A(V)$  as a function of the Coulomb potential  $U$ , ranging from the weak (a) to strong (b) hybridizations  $t_m$ . In the limit  $U \ll \Gamma_S$  these plots resemble the results shown in Fig. 3. Some qualitative changes appear at stronger interactions, especially on the doublet side  $U \geq \Gamma_S$ .

In absence of the Majorana mode we have shown [58], that differential conductance of the N-QD-S system is characterized by two peaks at the Andreev states and additional enhancement at zero-bias due to the Kondo effect, which operates only in the doublet region  $U \geq \Gamma_S$ . From the generalized Schrieffer-Wolff transformation we have estimated that  $\ln T_K \propto 1/\left[1 - \left(\frac{\Gamma_S}{U}\right)^2\right]$ , which yields a broadening caused by the on-dot pairing [58]. For  $U \gg \Gamma_S$  the Andreev scattering is quickly suppressed (because the off diagonal parts of Green's function disappear). In the present case a leakage of the Majorana quasiparticle obscures the mentioned behavior. For

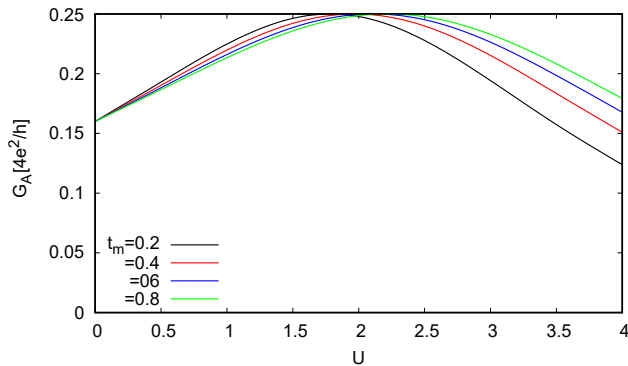


FIG. 7. The zero-bias Andreev conductance  $G_A(V=0)$  as a function of the Coulomb potential  $U$  (in units of  $\Gamma_N$ ) obtained for  $\epsilon = -U/2$ ,  $\Gamma_S = 2\Gamma_N$ ,  $\epsilon_m = 0$ .

$\Gamma_S \sim U$  we no longer observe any single peak structure, but rather a superposition of the induced Majorana feature (of a width dependent on  $t_m$ ) and the initial Kondo peak (whose width is strictly controlled by  $U/\Gamma_S$  ratio).

For larger voltages  $|V| \neq 0$  the differential conductance  $G_A(V)$  in the weak coupling  $t_m$  is similar to N-QD-S system. For strong coupling  $t_m$  we obtain the four-peak shape of  $G_A(V)$ . Internal peaks are related to the Andreev states, whereas the external ones are driven by the Majorana modes. With the increasing Coulomb potential the Andreev peaks merge into a single central peak and the side-peaks disappear.

Fig. 7 shows the linear conductance as a function of the Coulomb interaction. The optimal conductance approaches the value  $e^2/h$ , which is 4 times smaller than for the N-QD-S system without the side-attached Majorana mode (see Refs [62, 63]). Maximum of  $G_A(V=0)$  occurs at  $U \approx \Gamma_S$ , in a crossover between the BCS-type singlet and the doublet configurations [62]. In the present system (with  $t_m \neq 0$ ) the maximum of  $G_A(eV=0)$  moves towards larger values  $U > \Gamma_S$ , suggesting that the leaking Majorana mode competes with the Kondo state.

## VI. SUMMARY

We have analyzed the spin-resolved spectroscopic features of the correlated quantum dot side-coupled to the topologically superconducting nanowire, hosting the Majorana quasiparticles, focusing on STM-type geometry. Under such circumstances the subgap quasiparticles can be probed by the Andreev tunneling, involving simultaneously the particle and hole degrees of freedom.

In the uncorrelated case ( $U = 0$ ) a leakage of the Majorana quasiparticle induces either the zero-energy peak or dip in the QD spectral density, depending on the spin (Fig. 2). These effects originate from the constructive or destructive quantum interference, as can be inferred from the full counting statistics analysis [64]. We predict, that the differential Andreev conductance would be predominantly influenced by a destructive interference, leading

to the zero-bias dip feature preserved from the weak to strong hybridization  $t_m$  regimes.

We have also inspected the correlated quantum dot ( $U \neq 0$ ) case, studying an interplay between the Kondo effect and the Majorana quasiparticle. Coulomb interaction along with the proximity induced on-dot pairing can cause a transition from the spinless to the spinful configurations, manifested by a crossing of the Andreev/Shiba quasiparticles [53]. Finite coupling  $\Gamma_N$  with the STM tip could drive the virtual exchange between the QD and conducting electrons [34, 58], inducing the subgap Kondo effect [53]. We have found, that the side-attached Majorana quasiparticle gives rise to unusual behavior near this quantum phase transition/crossover.

Interplay of the subgap Kondo effect and Majorana quasiparticle shows up in the low-energy QD spectrum and in the tunneling conductance. In the weak correlation regime the Majorana state prevails, whereas in the strong correlation limit the Kondo physics plays a major role. The most interesting intermediate regime reveals completely novel signatures [60, 61, 65–68], without analogy to any known behavior. In the present context, we predict the linear conductance to be reduced to 25 % of its perfect value typical for N-QD-S junctions [53]. This results is in stark contrast from what has been predicted for N-QD-N junctions, where the single particle conductance is reduced to only 75 % of the unitary value [37]. In both cases, however, underlying mechanism is related to a fractional character of the Majorana quasiparticle.

We hope that the present analysis would encourage experimental attempts to realize the STM setup proposed in Fig. 1, that could reveal unusual physics driven by: electron pairing, strong correlations, and exotic nature of the Majorana quasiparticles.

## ACKNOWLEDGMENTS

This work is supported by the National Science Centre in Poland via project DEC-2014/13/B/ST3/04451 (TD) and the Faculty of Mathematics and Natural Sciences of the University of Rzeszów through the Project No. WMP/GD-06/2017 (GG).

## Appendix A: Short wire case

Main part of this paper is devoted to the infinitely long nanowire, where the edge Majorana do not overlap with each other ( $\epsilon_m = 0$ ). In such case the Kondo resonance and the Majorana quasiparticle are pinned to the Fermi level  $\mu_S$  of the superconducting lead, leading to competition between these effects [37, 50].

In the case of finite size nanowires the Majorana modes are characterized by a finite overlap ( $\epsilon_m \neq 0$ ). Under such circumstances for  $\Gamma_N = 0$  and  $U = 0$  we obtain six quasiparticle states: two of them being the Andreev bound states ( $\omega_{\pm} \pm \sqrt{\epsilon^2 + (\Gamma_S/2)^2}$ ) and the

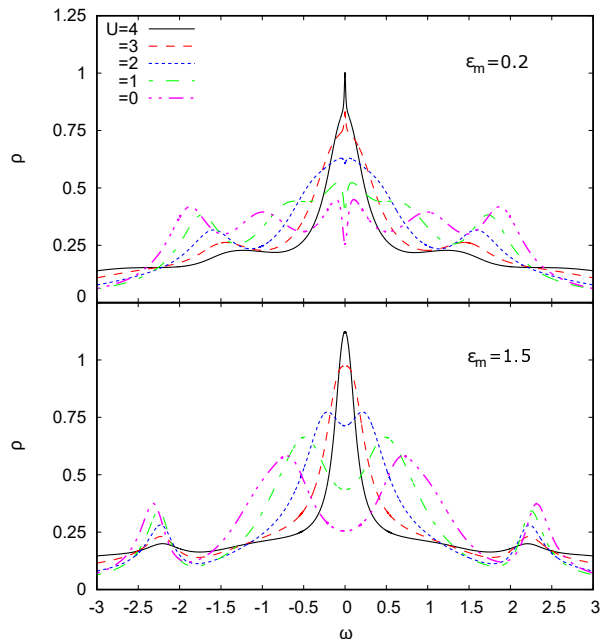


FIG. 8. The total spectral function  $\rho(\omega)$  of the correlated dot obtained for different values of  $U$ , using  $\Gamma_S = 2\Gamma_N$ ,  $\epsilon = -U/2$ ,  $t_m = 0.8$ ,  $\epsilon_m = 0.2$  (a) and  $\epsilon_m = 1.5$  (b).

other four states being related to Majorana quasiparticles  $\omega_{\pm} \pm (X/2 \pm 1/2\sqrt{X^2 - 4\epsilon_m^2(\epsilon^2 + \Gamma_S^2/4)})^{0.5}$ , where  $X = \epsilon^2 + \epsilon_m^2 + \Gamma_S^2/4 + 4t_m^2$ . In presence of correlations and for finite  $\Gamma_N \neq 0$  these quasiparticle states appear away from the Fermi energy, therefore their competition with the Kondo effect should be rather negligible. In Fig. 8 we present the total spectral function obtained for two values of  $\epsilon_m$  in the Kondo regime. For small  $\epsilon_m = 0.2$  (Fig. 8 (a)) and in the weak interaction limit we clearly observe six subgap quasiparticle peaks. With increasing  $U$  two of them merge into the Kondo resonance peak (for  $U \geq \Gamma_S$ ) with a tiny superstructure at  $\omega = 0$ . Contrary to such behavior, for large overlap  $\epsilon_m = 1.5$  (Fig. 8 (b)) we obtain the spectrum reminiscent of the N-QD-S system (see Fig. 5 (a)) with only some redistribution of the spectral weight at higher energies.

Finite overlap  $\epsilon_m$  has also influence on the differential Andreev conductance. In Fig. 9 we present  $G_A(V)$  as a function of the applied voltage  $V$  for the long ( $\epsilon_m = 0.2$ ) and short ( $\epsilon_m = 1.5$ ) nanowires, respectively. In the first case we observe well pronounced zero-bias peak which is characterized by a narrow width, controlled by  $\epsilon_m$ . Optimal value of the zero-bias peak approaches  $4e^2/h$  for  $U \approx \Gamma_S$ . For small  $U < \Gamma_S$  we observe two Andreev and two Majorana-Andreev hybridized peaks showing up in differential conductance. With the increasing Coulomb interaction  $U$  the Andreev peaks evolve into the central peak, appearing at  $V = 0$ . On the other hand, for the short nanowire ( $\epsilon_m = 1.5$ ) and at small voltages the dif-

ferential conductance  $G_A(eV)$  is similar as for N-QD-S system [58].

Fig. 10 shows the linear conductance  $G_A(V = 0)$

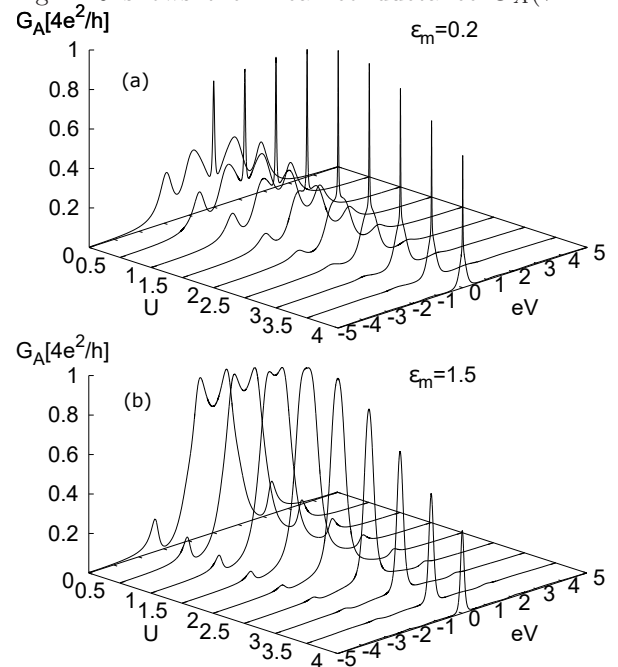


FIG. 9. The differential Andreev conductance  $G_A$  as a function of the applied voltage  $eV$  for  $\Gamma_S = 2\Gamma_N$ ,  $\epsilon = -U/2$ ,  $\epsilon_m = 0.2$  (a) and  $\epsilon_m = 1.5$  (b).

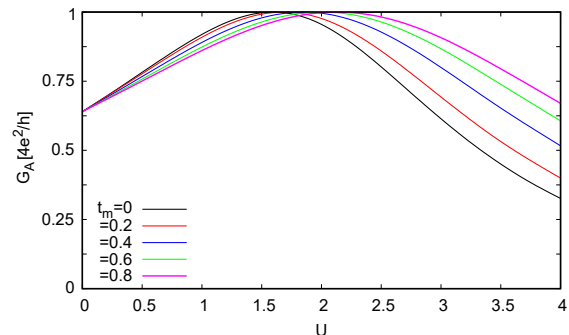


FIG. 10. The linear conductance  $G_A(V = 0)$  as a function of the Coulomb potential  $U$  for  $\Gamma_S = 2\Gamma_N$ ,  $\epsilon = -U/2$  and  $\epsilon_m = 0.2$ .

as a function of the Coulomb potential  $U$  obtained for  $\epsilon_m = 0.2$  and several values of the overlap  $t_m$ . We can notice, that optimal value of  $G_A(V = 0)$  is indeed  $4e^2/h$ , which occurs at the quantum phase transition (for the finite coupling  $\Gamma_N$  it is changed to a smooth crossover). For  $U > \Gamma_S$  the ground states evolves into the spinful doublet with a gradual suppression of the on-dot pairing, therefore the anomalous Andreev conductance  $G_A$  monotonously vanishes. For larger overlap  $t_m$  this changeover of the Andreev conductance slightly moves towards higher values of the Coulomb potential.

- 
- [1] J. Alicea, “New directions in the pursuit of Majorana fermions in solid state systems,” *Rep. Prog. Phys.* **75**, 076501 (2012).
- [2] M. Leijnse and K. Flensberg, “Introduction to topological superconductivity and Majorana fermions,” *Semicond. Sci. Technol.* **27**, 124003 (2012).
- [3] T. D. Stanescu and S. Tewari, “Majorana fermions in semiconductor nanowires: fundamentals, modeling, and experiment,” *J. Phys.: Condens. Matter* **25**, 233201 (2013).
- [4] C. W. J. Beenakker, “Search for Majorana fermions in superconductors,” *Annu. Rev. Condens. Matter Phys.* **4**, 113 (2013).
- [5] S. R. Elliott and M. Franz, “Colloquium: Majorana fermions in nuclear, particle, and solid-state physics,” *Rev. Mod. Phys.* **87**, 137 (2015).
- [6] G. E. Volovik, “Fermion zero modes on vortices in chiral superconductors,” *JETP Lett.* **70**, 609 (1999).
- [7] N. Read and D. Green, “Paired states of fermions in two dimensions with breaking of parity and time-reversal symmetries and the fractional quantum Hall effect,” *Phys. Rev. B* **61**, 10267 (2000).
- [8] A. Y. Kitaev, “Unpaired Majorana fermions in quantum wires,” *Phys. Usp.* **44**, 131 (2001).
- [9] X. Liu, X. Li, D.-L. Deng, X.-J. Liu, and S. Das Sarma, “Majorana spintronics,” *Phys. Rev. B* **94**, 014511 (2016).
- [10] S. Tewari, S. Das Sarma, C. Nayak, C. Zhang, and P. Zoller, “Quantum computation using vortices and Majorana zero modes of a  $p_x + ip_y$  superfluid of fermionic cold atoms,” *Phys. Rev. Lett.* **98**, 010506 (2007).
- [11] L. Fu and C. L. Kane, “Superconducting proximity effect and Majorana fermions at the surface of a topological insulator,” *Phys. Rev. Lett.* **100**, 096407 (2008).
- [12] J. Nilsson, A. R. Akhmerov, and C. W. J. Beenakker, “Splitting of a Cooper pair by a pair of Majorana bound states,” *Phys. Rev. Lett.* **101**, 120403 (2008).
- [13] M. Sato and S. Fujimoto, “Topological phases of noncentrosymmetric superconductors: Edge states, Majorana fermions, and non-Abelian statistics,” *Phys. Rev. B* **79**, 094504 (2009).
- [14] M. Wimmer, A. R. Akhmerov, M. V. Medvedyeva, J. Tworzydło, and C. W. J. Beenakker, “Majorana bound states without vortices in topological superconductors with electrostatic defects,” *Phys. Rev. Lett.* **105**, 046803 (2010).
- [15] J. D. Sau, R. M. Lutchyn, S. Tewari, and S. Das Sarma, “Generic new platform for topological quantum computation using semiconductor heterostructures,” *Phys. Rev. Lett.* **104**, 040502 (2010).
- [16] Y. Oreg, G. Refael, and F. von Oppen, “Helical liquids and Majorana bound states in quantum wires,” *Phys. Rev. Lett.* **105**, 177002 (2010).
- [17] R. M. Lutchyn, J. D. Sau, and S. Das Sarma, “Majorana fermions and a topological phase transition in semiconductor-superconductor heterostructures,” *Phys. Rev. Lett.* **105**, 077001 (2010).
- [18] T.-P. Choy, J. M. Edge, A. R. Akhmerov, and C. W. J. Beenakker, “Majorana fermions emerging from magnetic nanoparticles on a superconductor without spin-orbit coupling,” *Phys. Rev. B* **84**, 195442 (2011).
- [19] L. Jiang, T. Kitagawa, J. Alicea, A. R. Akhmerov, D. Pekker, G. Refael, J. I. Cirac, E. Demler, M. D. Lukin, and P. Zoller, “Majorana fermions in equilibrium and in driven cold-atom quantum wires,” *Phys. Rev. Lett.* **106**, 220402 (2011).
- [20] P. San-Jose, E. Prada, and R. Aguado, “ac Josephson effect in finite-length nanowire junctions with Majorana modes,” *Phys. Rev. Lett.* **108**, 257001 (2012).
- [21] V. Mourik, K. Zuo, S. M. Frolov, S. R. Plissard, E. P. A. M. Bakkers, and L. P. Kouwenhoven, “Signatures of Majorana fermions in hybrid superconductor-semiconductor nanowire devices,” *Science* **336**, 1003 (2012).
- [22] H. Zhang et al., “Ballistic Majorana nanowire devices,” (2016), arXiv:1603.04069.
- [23] S. Nadj-Perge, I. K. Drozdov, J. Li, H. Chen, S. Jeon, J. Seo, A. H. MacDonald, B. A. Bernevig, and A. Yazdani, “Observation of Majorana fermions in ferromagnetic atomic chains on a superconductor,” *Science* **346**, 602 (2014).
- [24] R. Pawlak, M. Kisiel, J. Klinovaja, T. Maier, S. Kawai, T. Glatzel, D. Loss, and E. Meyer, “Probing atomic structure and Majorana wave-functions in mono-atomic Fe-chains on superconducting Pb-surface,” *npj Quantum Info* **2**, 16035 (2016).
- [25] M. Ruby, F. Pientka, Y. Peng, F. von Oppen, B. W. Heinrich, and K. J. Franke, “End states and subgap structure in proximity-coupled chains of magnetic adatoms,” *Phys. Rev. Lett.* **115**, 197204 (2015).
- [26] S. Jeon, Y. Xie, J. Li, Z. Wang, B. A. Bernevig, and A. Yazdani, “Distinguishing a Majorana zero mode using spin-resolved measurements,” *Science* (2017), 10.1126/science.aan3670.
- [27] M. T. Deng, S. Vaitiekenas, E. B. Hansen, J. Danon, M. Leijnse, K. Flensberg, J. Nygård, P. Krogstrup, and C. M. Marcus, “Majorana bound state in a coupled quantum-dot hybrid-nanowire system,” *Science* **354**, 1557 (2016).
- [28] C.-X. Liu, J. D. Sau, T. D. Stanescu, and S. Das Sarma, “Andreev bound states versus Majorana bound states in quantum dot-nanowire-superconductor hybrid structures: Trivial versus topological zero-bias conductance peaks,” *Phys. Rev. B* **96**, 075161 (2017).
- [29] S. Hoffman, D. Chevallier, D. Loss, and J. Klinovaja, “Spin-dependent coupling between quantum dots and topological quantum wires,” *Phys. Rev. B* **96**, 045440 (2017).
- [30] A. Ptok, A. Kobińska, and T. Domański, “On controlling the bound states in quantum-dot hybrid-nanowire,” (2017), arXiv:1710.06387.
- [31] E. Prada, R. Aguado, and P. San-Jose, “Measuring Majorana nonlocality and spin structure with a quantum dot,” *Phys. Rev. B* **96**, 085418 (2017).
- [32] J. Barański, A. Kobińska, and T. Domański, “Spin-sensitive interference due to Majorana state on the interface between normal and superconducting leads,” *J. Phys.: Condens. Matter* **29**, 075603 (2017).
- [33] R. Chirla and C. P. Moca, “Fingerprints of Majorana fermions in spin-resolved subgap spectroscopy,” *Phys. Rev. B* **94**, 045405 (2016).
- [34] R. Žitko, J. Soo Lim, R. López, and R. Aguado,

- “Shiba states and zero-bias anomalies in the hybrid normal-superconductor Anderson model,” *Phys. Rev. B* **91**, 045441 (2015).
- [35] D. E. Liu and H. U. Baranger, “Detecting a Majorana-fermion zero mode using a quantum dot,” *Phys. Rev. B* **84**, 201308 (2011).
- [36] R. López, M. Lee, L. Serra, and J. S. Lim, “Thermoelectrical detection of Majorana states,” *Phys. Rev. B* **89**, 205418 (2014).
- [37] M. Lee, J. S. Lim, and R. López, “Kondo effect in a quantum dot side-coupled to a topological superconductor,” *Phys. Rev. B* **87**, 241402 (2013).
- [38] Y. Cao, P. Wang, G. Xiong, M. Gong, and X.-Q. Li, “Probing the existence and dynamics of Majorana fermion via transport through a quantum dot,” *Phys. Rev. B* **86**, 115311 (2012).
- [39] E. Vernek, P. H. Penteado, A. C. Seridonio, and J. C. Egues, “Subtle leakage of a Majorana mode into a quantum dot,” *Phys. Rev. B* **89**, 165314 (2014).
- [40] W.-J. Gong, S.-F. Zhang, Z.-C. Li, G. Yi, and Y.-S. Zheng, “Detection of a Majorana fermion zero mode by a T-shaped quantum-dot structure,” *Phys. Rev. B* **89**, 245413 (2014).
- [41] D. E. Liu, M. Cheng, and R. M. Lutchyn, “Probing Majorana physics in quantum-dot shot-noise experiments,” *Phys. Rev. B* **91**, 081405 (2015).
- [42] P. Stefański, “Signatures of Majorana states in electron transport through a quantum dot coupled to topological wire,” *Acta Phys. Pol. A* **127**, 198 (2015).
- [43] Z.-Z. Li, C.-H. Lam, and J. Q. You, “Probing Majorana bound states via counting statistics of a single electron transistor,” *Sci. Rep.* **5**, 11416 (2015).
- [44] I. Weymann, “Spin Seebeck effect in quantum dot side-coupled to topological superconductor,” *J. Phys.: Condens. Matter* **29**, 095301 (2017).
- [45] I. Weymann and K. P. Wójcik, “Transport properties of a hybrid Majorana wire-quantum dot system with ferromagnetic contacts,” *Phys. Rev. B* **95**, 155427 (2017).
- [46] S.-X. Wang, Y.-X. Li, N. Wang, and J.-J. Liu, “Andreev reflection in a T-shaped double quantum-dot with coupled Majorana bound states,” *Acta Phys. Sin.* **65**, 137302 (2016).
- [47] A. V. Balatsky, I. Vekhter, and J.-X. Zhu, “Impurity-induced states in conventional and unconventional superconductors,” *Rev. Mod. Phys.* **78**, 373 (2006).
- [48] T. Domański, “Particle-hole mixing driven by the superconducting fluctuations,” *Eur. Phys. J. B* **74**, 437 (2010).
- [49] A. Golub, “Multiple Andreev reflections in *s*-wave superconductor-quantum dot-topological superconductor tunnel junctions and Majorana bound states,” *Phys. Rev. B* **91**, 205105 (2015).
- [50] D. A. Ruiz-Tijerina, E. Vernek, L. G. G. V. Dias da Silva, and J. C. Egues, “Interaction effects on a Majorana zero mode leaking into a quantum dot,” *Phys. Rev. B* **91**, 115435 (2015).
- [51] J. Bauer, A. Oguri, and A. C. Hewson, “Spectral properties of locally correlated electrons in a Bardeen-Cooper-Schrieffer superconductor,” *J. Phys.: Condens. Matter* **19**, 486211 (2007).
- [52] Y. Yamada, Y. Tanaka, and N. Kawakami, “Interplay of Kondo and superconducting correlations in the nonequilibrium Andreev transport through a quantum dot,” *Phys. Rev. B* **84**, 075484 (2011).
- [53] A. Martín-Rodero and A. Levy Yeyati, “Josephson and Andreev transport through quantum dots,” *Advances in Physics* **60**, 899 (2011).
- [54] J. Barański and T. Domański, “In-gap states of a quantum dot coupled between a normal and a superconducting lead,” *J. Phys.: Condens. Matter* **25**, 435305 (2013).
- [55] A. F. Andreev, “The thermal conductivity of the intermediate state in superconductors,” *J. Exp. Theor. Phys* **19**, 1228 (1964).
- [56] E. Vecino, A. Martín-Rodero, and A. Levy Yeyati, “Josephson current through a correlated quantum level: Andreev states and  $\pi$  junction behavior,” *Phys. Rev. B* **68**, 035105 (2003).
- [57] A. Martín-Rodero and A. Levy Yeyati, “The Andreev states of a superconducting quantum dot: mean field versus exact numerical results,” *J. Phys.: Condens. Matter* **24**, 385303 (2012).
- [58] T. Domański, I. Weymann, M. Barańska, and G. Górski, “Constructive influence of the induced electron pairing on the Kondo state,” *Sci. Rep.* **6**, 23336 (2016).
- [59] T. Domański, M. Žonda, V. Pokorný, G. Górski, V. Janiš, and T. Novotný, “Josephson-phase-controlled interplay between correlation effects and electron pairing in a three-terminal nanostructure,” *Phys. Rev. B* **95**, 045104 (2017).
- [60] M. Cheng, M. Becker, B. Bauer, and R. M. Lutchyn, “Interplay between Kondo and Majorana interactions in quantum dots,” *Phys. Rev. X* **4**, 031051 (2014).
- [61] I. J. van Beek and B. Braunecker, “Non-Kondo many-body physics in a Majorana-based Kondo type system,” *Phys. Rev. B* **94**, 115416 (2016).
- [62] Y. Tanaka, N. Kawakami, and A. Oguri, “Numerical renormalization group approach to a quantum dot coupled to normal and superconducting leads,” *J. Phys. Soc. Japan* **76**, 074701 (2007).
- [63] G. Górski, “Irreducible Green functions method applied to nanoscopic systems,” *Acta Phys. Pol.* **130**, 551 (2016).
- [64] A. Schuray, L. Weithofer, and P. Recher, “Fano resonances in majorana bound state-quantum dot hybrid systems,” *Phys. Rev. B* **96**, 085417 (2017).
- [65] B. Béri and N. R. Cooper, “Topological kondo effect with majorana fermions,” *Phys. Rev. Lett.* **109**, 156803 (2012).
- [66] M. R. Galpin, A. K. Mitchell, J. Temaismithi, D. E. Logan, B. Béri, and N. R. Cooper, “Conductance fingerprint of majorana fermions in the topological kondo effect,” *Phys. Rev. B* **89**, 045143 (2014).
- [67] S. Plugge, A. Zazunov, E. Eriksson, A. M. Tsvelik, and R. Egger, “Kondo physics from quasiparticle poisoning in majorana devices,” *Phys. Rev. B* **93**, 104524 (2016).
- [68] B. Béri, “Exact nonequilibrium transport in the topological kondo effect,” *Phys. Rev. Lett.* **119**, 027701 (2017).